arXiv:1601.07938v2 [cond-mat.mtrl-sci] 20 Feb 2016

Computing forces on interface elements exerted by dislocations in an elastically anisotropic crystalline material

B. Liu[1,*], A. Arsenlis[1], S. Aubry[1]

[1]Lawrence Livermore National Laboratory, Livermore, CA 94550, USA
[*]Corresponding author: bingliu@llnl.gov (B. Liu)

February 23, 2016

Abstract

Driven by the growing interest in numerical simulations of dislocation–interface interactions in general crystalline materials with elastic anisotropy, we develop algorithms for the integration of interface tractions needed to couple dislocation dynamics with a finite element or boundary element solver. The dislocation stress fields in elastically anisotropic media are made analytically accessible through the spherical harmonics expansion of the derivative of Green's function, and analytical expressions for the forces on interface elements are derived by analytically integrating the spherical harmonics series recursively. Compared with numerical integration by Gaussian quadrature, the newly developed analytical algorithm for interface traction integration is highly beneficial in terms of both computation precision and speed.

Keywords: Dislocation dynamics; anisotropic elasticity; finite domain; interface traction integration; analytical solution

1 Introduction

It is well known that a dislocation approaching a free surface experiences an attractive force, so called image force [1]. In multiphase materials or single-phase elastically anisotropic polycrystalline materials, a dislocation near a phase or grain boundary is subject to a similar force due to the change in elasticity across the interface, which can be either attractive or repulsive [2–4]. As the magnitudes of these forces are inversely proportional to the dislocation–interface

distance, the effect of free surfaces on dislocation motion and multiplication becomes significant in submicrometre-sized crystals [5–8], and the elastic interactions between dislocations and phase/grain boundaries have a stronger impact on the mechanical properties of the nanostructured materials [9–12] than those of their coarse-grained counterparts.

For free surfaces and phase/grain boundaries of elastically anisotropic half spaces, such virtual forces (negative energy gradients) can be determined through the image force theorem of Barnett and Lothe [13–17]. For finite domains of more complex shapes, this problem of elastic interactions between dislocations and interfaces can only be solved through the coupling of a dislocation dynamics (DD) code and a finite element (FE) or boundary element (BE) solver [18–28]. In such cases, the stress field of the dislocation in an infinite elastically homogeneous medium is used to calculate the traction on the surface bounding the elastic solid, and then correction fields are added to impose the proper boundary conditions on the domain. For free surfaces this results in an imposition of an equal and opposite surface traction such that the net result is a zero traction condition, and for phase/grain boundaries there is a traction balance and displacement continuity condition that must be imposed. This work is focused on the first part of DD-FE/BE simulations of dislocation–interface interactions, i.e. determination of forces on interface elements due to tractions imposed by dislocations in an infinite elastically anisotropic medium.

Interface tractions exerted by dislocation stress fields must be integrated into nodal forces in a FE or BE solver. These nodal forces are surface integrals of the traction field $\boldsymbol{T}$ (force per unit area) over the individual interface FE or BE elements [20, 24, 28],

$$\boldsymbol{F}^{(n)} = \int_S \boldsymbol{T}\left(\boldsymbol{x}\right) N_S^{(n)}(\boldsymbol{x})\mathrm{d}S = \int_S \left[\boldsymbol{\sigma}\left(\boldsymbol{x}\right)\cdot\boldsymbol{n}\right] N_S^{(n)}(\boldsymbol{x})\mathrm{d}S, \tag{1}$$

where $\boldsymbol{F}^{(n)}$ is the force on a FE or BE node n of an interface element S exerted by dislocation stress field $\boldsymbol{\sigma}\left(\boldsymbol{x}\right)$, $\boldsymbol{n}$ is the interface normal, and $N_s^{(n)}(\boldsymbol{x})$ are the FE or BE shape functions. In this paper, we will refer to these nodal forces as traction forces. The traction force on a FE or BE node is analogous to the interaction force due to dislocation stress field on a dislocation node in nodal based (one-dimensional FE) dislocation dynamics models [20, 29–31]. The dislocation interaction forces are line integrals of the Peach-Koehler force $\boldsymbol{f}^{PK}$ (force per unit length) along the individual dislocation segments [20, 31],

$$\boldsymbol{f}^{(n)} = \int_L \boldsymbol{f}^{PK}\left(\boldsymbol{x}\right) N_L^{(n)}(\boldsymbol{x})\mathrm{d}L = \int_L \left[\boldsymbol{\sigma}\left(\boldsymbol{x}\right)\cdot\boldsymbol{b}\times\boldsymbol{t}\right] N_L^{(n)}(\boldsymbol{x})\mathrm{d}L, \tag{2}$$

where $\boldsymbol{f}^{(n)}$ is the force on a node n of a dislocation segment L exerted by dislocation stress field $\boldsymbol{\sigma}\left(\boldsymbol{x}\right)$, with $\boldsymbol{b}$, $\boldsymbol{t}$, and $N_L^{(n)}(\boldsymbol{x})$ being the Burgers vector, line direction, and shape function of the dislocation segment, respectively. While the dislocation interaction force calculation is the core of a DD model, the interface traction force evaluation is the main link in DD-FE/BE finite domain simulations. However, the compromise between accuracy and efficiency of the numerical integrations of dislocation interaction forces and surface traction forces has been the bottleneck for large-scale DD simulations [31] and DD–FE/BE simulations of the elastic interactions between dislocations and free surfaces [20, 24, 32–34]. Due to the limitations of numerical integrations, an alternative analytical integration of interface traction forces is highly desirable.

For isotropic elastic media, the stress field of a dislocation loop can be calculated analytically through line integrations of the derivatives of Green's function along piecewise straight dislocation segments [35, 36]. Arsenlis et al. [31] developed analytical expressions for dislocation interaction force calculations that involves double integrations along the individual pairs of interacting dislocation segments, i.e. the first line integration along the source segment to get its stress field and the second line integration along the receiving segment to obtain the interaction force. These analytical expressions for dislocation interaction force calculations have already been used in many DD simulations, e.g. discovery of ternary dislocation junctions in body-centered cubic metals [37], interpretation of the size-dependent strength for micrometer-sized crystals [38], determination of low-angle grain boundary penetration resistances [39, 40], observation of strain localization via defect-free channels in highly irradiated materials [41], and revealing the mechanisms of dynamic recovery during high temperature creep of single-crystal superalloys [42]. Queyreau et al. [43] have recently formulated analytical expressions to calculate surface traction forces induced by stress field of a dislocation in isotropic elastic media for rectangular surface elements, which give the precise solutions to triple integrals, i.e. one integral along the dislocation segments for the stress field and then a double integral over the surface element to obtain the traction force.

In anisotropic elasticity theory of dislocations, the analytical expression for the stress field of an arbitrary dislocation loop does not exist [44, 45]. The dislocation stress field calculation based on Stroh's formulism [35, 46] requires numerical integrations [47, 48] or solving an eigenvalue problem for a six by six matrix [48] to obtain the associated matrices and their angular derivatives. The dislocation stress field computations using Mura's formula [49] has relied on direct numerical integrations of the derivatives of Green's function [50]. Recently, Aubry and Arsenlis [51] used a truncated spherical harmonics expansion to approximate the derivatives of Green's function, and have analytically integrated the spherical harmonics series to calculate dislocation stress field (single integrals) and interaction force (double integrals) for straight dislocation segments. In this work, we use the same spherical harmonics expansion of the derivatives of Green's function formulated in the previous work [51], and analytically integrate the associated spherical harmonics series to determine the interface traction force (triple integrals) in anisotropic elastic media for quadrilateral surface elements.

2 Method

In a homogeneous infinite linear elastic solid, the stress field of a dislocation loop can be expressed in terms of a contour integral along the loop [49],

$$\sigma_{js}\left(\boldsymbol{x}\right) = \epsilon_{ngr} C_{jsvg} C_{pdwn} b_w \oint_L \frac{\partial G_{vp}}{\partial x_d}\left(\boldsymbol{x} - \boldsymbol{x}'\right) \mathrm{d}x'_r, \tag{3}$$

where C_{ijkl} is the elastic stiffness tensor, ϵ is the permutation tensor, $\boldsymbol{b}$ is the Burgers vector of the dislocation loop, and $\partial G_{vp}/\partial x_d$ is the derivative of the Green's function $G_{vp}\left(\boldsymbol{x} - \boldsymbol{x}'\right)$, which is defined as the displacement in the x_v-direction at point $\boldsymbol{x}$ in response to a unit point force in the x_p-direction applied at point $\boldsymbol{x}'$.

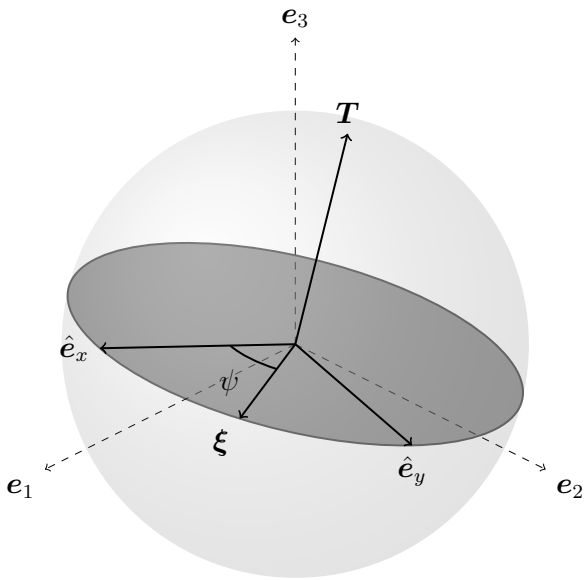

Figure 1: Unit sphere in anisotropic elasticity

The Green's function in an anisotropic elastic medium has been obtained as a single integral [44],

$$G_{vp} = \frac{1}{4\pi^2 R} \int_0^\pi M_{vp}^{-1}(\xi)\, \mathrm{d}\psi, \tag{4}$$

where

$$M_{vp}^{-1}(\xi) = \frac{\epsilon_{vsm}\epsilon_{prw}(\xi\xi)_{sr}(\xi\xi)_{mw}}{2\epsilon_{lgn}(\xi\xi)_{1l}(\xi\xi)_{2g}(\xi\xi)_{3n}},$$

with the notation $(\xi\xi)_{ij} = \xi_k C_{kijl}\xi_l$. R is the norm of vector $\boldsymbol{R} = \boldsymbol{x} - \boldsymbol{x}'$, i.e. $R = \|\boldsymbol{R}\|$. $\boldsymbol{T}$ is the direction of vector $\boldsymbol{R}$, i.e. $\boldsymbol{T} = \boldsymbol{R}/R$. ξ is a unit vector that varies in the plane $\boldsymbol{\xi} \cdot \boldsymbol{T} = 0$, $\hat{\boldsymbol{e}}_x$ and $\hat{\boldsymbol{e}}_y$ are two orthogonal unit vectors in the same plane, and the angle between $\hat{\boldsymbol{e}}_x$ and ξ is ψ, Fig. 1.

The corresponding integral expression for the derivative of Green's function is [52],

$$\frac{\partial G_{vp}}{\partial x_d} = \frac{1}{4\pi^2 R^2} \int_0^\pi \left(-T_d M_{vp}^{-1} + \xi_d N_{vp}\right) \mathrm{d}\psi, \tag{5}$$

where $N_{vp} = C_{jrnw} M_{vj}^{-1} M_{np}^{-1} (\xi_r T_w + \xi_w T_r)$. See the overview of Bacon et al. [44] for more details.

The derivative of the Green's function is a product of a part depending only on $1/R^2$ and an angular part $\boldsymbol{g}$ depending only on the direction $\boldsymbol{T}$

$$g_{vpd}(\boldsymbol{T}) = g_{vpd}(\theta, \phi) = \int_0^\pi \left(-T_d M_{vp}^{-1} + \xi_d N_{vp}\right) \mathrm{d}\psi, \tag{6}$$

where (θ, ϕ) are the spherical coordinates of $\boldsymbol{T}$.

There is no analytical expression for g_{vpd}, but the function $g_{vpd}\left(\boldsymbol{T}\right)$ is suitable for decomposition in spherical harmonics.

$$\boldsymbol{g}\left(\boldsymbol{T}\right)=\sum_{l=0}^{\infty}\sum_{m=-l}^{l}\boldsymbol{g}^{lm}Y_{l}^{m}\left(\boldsymbol{T}\right) \tag{7}$$

The expansion coefficients $\boldsymbol{g}^{lm}$ are independent of $\boldsymbol{T}\left(\theta,\phi\right)$, and are defined as

$$\boldsymbol{g}^{lm}=\int_{0}^{2\pi}\int_{0}^{\pi}\boldsymbol{g}\left(\theta,\phi\right)Y_{l}^{m*}\left(\theta,\phi\right)\sin\theta\mathrm{d}\theta\mathrm{d}\phi \tag{8}$$

The spherical harmonics Y_l^m are defined as the complex functions

$$Y_{l}^{m}(\theta,\phi)=\sqrt{\frac{2l+1}{4\pi}\frac{(l-m)!}{(l+m)!}}\,P_{l}^{m}(\cos\theta)\,e^{im\phi}, \tag{9}$$

where P_l^m are the associated Legendre polynomials. To be consistent with the definition of elastic stiffness tensor C_{ijkl}, we rewrite Y_l^m in the Cartesian coordinate system $(\boldsymbol{e}_1,\boldsymbol{e}_2,\boldsymbol{e}_3)$, i.e. $x=\boldsymbol{T}\cdot\boldsymbol{e}_1$, $y=\boldsymbol{T}\cdot\boldsymbol{e}_2$, and $z=\boldsymbol{T}\cdot\boldsymbol{e}_3$, in the form of

$$Y_{l}^{m}(x,y,z)=f_{m}(x,y)\sum_{k=0}^{[(l-|m|)/2]}\bar{Q}_{l}^{|m|}(k)z^{l-|m|-2k} \tag{10}$$

where

$$f_{m}(x,y)=\begin{cases}(x+iy)^{m} & m\geq0\\(x-iy)^{-m} & m<0\end{cases}$$

and

$$\bar{Q}_{l}^{m}(k)=\frac{(-1)^{m+k}}{4\pi^{2}}\frac{m!}{2^{l}}\sqrt{\frac{2l+1}{4\pi}\frac{(l-m)!}{(l+m)!}}\begin{pmatrix}l\\k\end{pmatrix}\begin{pmatrix}2l-2k\\l\end{pmatrix}\begin{pmatrix}l-2k\\m\end{pmatrix}$$

The function $\boldsymbol{g}$ can then be defined as

$$\boldsymbol{g}(x,y,z)=\sum_{l=0}^{\infty}\sum_{m=0}^{l}\Re\left((x+iy)^{m}\boldsymbol{g}^{lm}\right)\sum_{k=0}^{[(l-m)/2]}Q_{l}^{m}(k)z^{l-m-2k} \tag{11}$$

where we note $\Re(x)$ is the real part of x, $Q_l^0(k)=\bar{Q}_l^0(k)$ when $m=0$, and $Q_l^m(k)=2\bar{Q}_l^m(k)$ when $m>0$.

Using the spherical harmonics series expansion of its angular part and defining $\boldsymbol{e}_{12}=\boldsymbol{e}_1+i\boldsymbol{e}_2$ with $x+iy=\frac{\boldsymbol{R}}{R}\cdot\boldsymbol{e}_{12}$ and $z=\frac{\boldsymbol{R}}{R}\cdot\boldsymbol{e}_3$, the derivative of the Green's function can be evaluated by

$$\frac{\partial G_{vp}}{\partial x_{d}}(\boldsymbol{R})=\sum_{l=0}^{\infty}\sum_{m=0}^{l}\sum_{k=0}^{[(l-m)/2]}\Re\left(Q_{l}^{m}(k)g_{vpd}^{lm}\frac{(\boldsymbol{R}\cdot\boldsymbol{e}_{12})^{m}(\boldsymbol{R}\cdot\boldsymbol{e}_{3})^{l-m-2k}}{R^{l-2k+2}}\right). \tag{12}$$

This definition involves a quotient of terms that are a function of R, which depends only on two variables m and $l-2k$. It can be simplified further to obtain

$$\frac{\partial G_{vp}}{\partial x_d}(\boldsymbol{R}) = \sum_{q=0}^{\infty}\sum_{m=0}^{2q+1} \Re\left(S_{vpd}^{qm}\frac{(\boldsymbol{R}\cdot\boldsymbol{e}_{12})^m(\boldsymbol{R}\cdot\boldsymbol{e}_3)^{2q+1-m}}{R^{2q+3}}\right) \tag{13}$$

where S_{vpd}^{qm} is a sum of products composed of $Q_l^m(k)$ and g_{vpd}^{lm}. The Green's function and its derivatives depend only on odd powers of $1/R$. This property means that in the spherical harmonics expansion, the non-zero terms correspond to the odd powers of $1/R$.

Within linear elasticity, the total stress field of a dislocation network is a superposition of the stress fields of individual dislocation segments in the network. For a straight dislocation segment linking two nodes at Cartesian coordinates $\boldsymbol{x}_1$ and $\boldsymbol{x}_2$, respectively, its stress field in an anisotropic elastic medium can then be expressed by

$$\sigma_{js}(\boldsymbol{x}) = \epsilon_{ngr}C_{jsvg}C_{pdwn}b_w\sum_{q=0}^{\infty}\sum_{m=0}^{2q+1}\Re\left(S_{vpd}^{qm}\int_{\boldsymbol{x}_1}^{\boldsymbol{x}_2}\frac{(\boldsymbol{R}\cdot\boldsymbol{e}_{12})^m(\boldsymbol{R}\cdot\boldsymbol{e}_3)^{2q+1-m}}{R^{2q+3}}\mathrm{d}x_r'\right) \tag{14}$$

Consider a quadrilateral element delimited by its Cartesian coordinates $\boldsymbol{x}_3$, $\boldsymbol{x}_4$, $\boldsymbol{x}_5$, and $\boldsymbol{x}_6$ as shown in Fig. 2, where $\boldsymbol{x}$ is the coordinate that spans within the element, and $\boldsymbol{x}'$ is the coordinate that spans along the dislocation segment delimited by $\boldsymbol{x}_1$ and $\boldsymbol{x}_2$. The vector $\boldsymbol{R}=\boldsymbol{x}-\boldsymbol{x}'$ can be rewritten as $\boldsymbol{R}=y\boldsymbol{t}+r\boldsymbol{p}+s\boldsymbol{q}$, with $\boldsymbol{t}=\frac{\boldsymbol{x}_2-\boldsymbol{x}_1}{\|\boldsymbol{x}_2-\boldsymbol{x}_1\|}$, $\boldsymbol{p}=\frac{\boldsymbol{x}_4-\boldsymbol{x}_3}{\|\boldsymbol{x}_4-\boldsymbol{x}_3\|}$, and $\boldsymbol{q}=\frac{\boldsymbol{x}_5-\boldsymbol{x}_3}{\|\boldsymbol{x}_5-\boldsymbol{x}_3\|}$.

Using $\boldsymbol{n}=\frac{\boldsymbol{p}\times\boldsymbol{q}}{\|\boldsymbol{p}\times\boldsymbol{q}\|}$ and $\mathrm{d}S=\|\boldsymbol{p}\times\boldsymbol{q}\|\mathrm{d}r\mathrm{d}s$, with a linear shape function in the form of a four-term polynomial $N^{(n)}(\boldsymbol{x})=a_0+a_1r+a_2s+a_3rs$, the traction force $\boldsymbol{F}^{(n)}$ can be expressed as

$$\boldsymbol{F}^{(n)} = \int_{s_1}^{s_2}\int_{r_1}^{r_2}\boldsymbol{\sigma}(\boldsymbol{x})\cdot(\boldsymbol{p}\times\boldsymbol{q})(a_0+a_1r+a_2s+a_3rs)\mathrm{d}r\mathrm{d}s \tag{15}$$

Combining Eq. (14) and Eq. (15) with $\mathrm{d}\boldsymbol{x}'=-\boldsymbol{t}\mathrm{d}y$, the interface nodal force due to dislocation traction in an anisotropic elastic medium can be determined through

$$\begin{aligned} F_j^{(n)} \;=\; & -t_r\epsilon_{sab}p_aq_b\epsilon_{ngr}C_{jsvg}C_{pdwn}b_w\textstyle\sum_{q=0}^{\infty}\sum_{m=0}^{2q+1} \\ & \Re\left(S_{vpd}^{qm}\textstyle\int_{s_1}^{s_2}\int_{r_1}^{r_2}\int_{y_1}^{y_2}\frac{(\boldsymbol{R}\cdot\boldsymbol{e}_{12})^m(\boldsymbol{R}\cdot\boldsymbol{e}_3)^{2q+1-m}}{R^{2q+3}}(a_0+a_1r+a_2s+a_3rs)\mathrm{d}y\mathrm{d}r\mathrm{d}s\right) \end{aligned} \tag{16}$$

The unknown parts of Eq. (16) are the following series of integrals:

$$\begin{aligned} K_{ijk} &= \int_{s_1}^{s_2}\int_{r_1}^{r_2}\int_{y_1}^{y_2}\frac{(\boldsymbol{R}\cdot\boldsymbol{e}_{12})^i(\boldsymbol{R}\cdot\boldsymbol{e}_3)^j}{R^k}\mathrm{d}y\mathrm{d}r\mathrm{d}s \\ K_{ijk}^r &= \int_{s_1}^{s_2}\int_{r_1}^{r_2}\int_{y_1}^{y_2}\frac{(\boldsymbol{R}\cdot\boldsymbol{e}_{12})^i(\boldsymbol{R}\cdot\boldsymbol{e}_3)^j}{R^k}r\mathrm{d}y\mathrm{d}r\mathrm{d}s \\ K_{ijk}^s &= \int_{s_1}^{s_2}\int_{r_1}^{r_2}\int_{y_1}^{y_2}\frac{(\boldsymbol{R}\cdot\boldsymbol{e}_{12})^i(\boldsymbol{R}\cdot\boldsymbol{e}_3)^j}{R^k}s\mathrm{d}y\mathrm{d}r\mathrm{d}s \\ K_{ijk}^{rs} &= \int_{s_1}^{s_2}\int_{r_1}^{r_2}\int_{y_1}^{y_2}\frac{(\boldsymbol{R}\cdot\boldsymbol{e}_{12})^i(\boldsymbol{R}\cdot\boldsymbol{e}_3)^j}{R^k}rs\mathrm{d}y\mathrm{d}r\mathrm{d}s, \end{aligned}$$

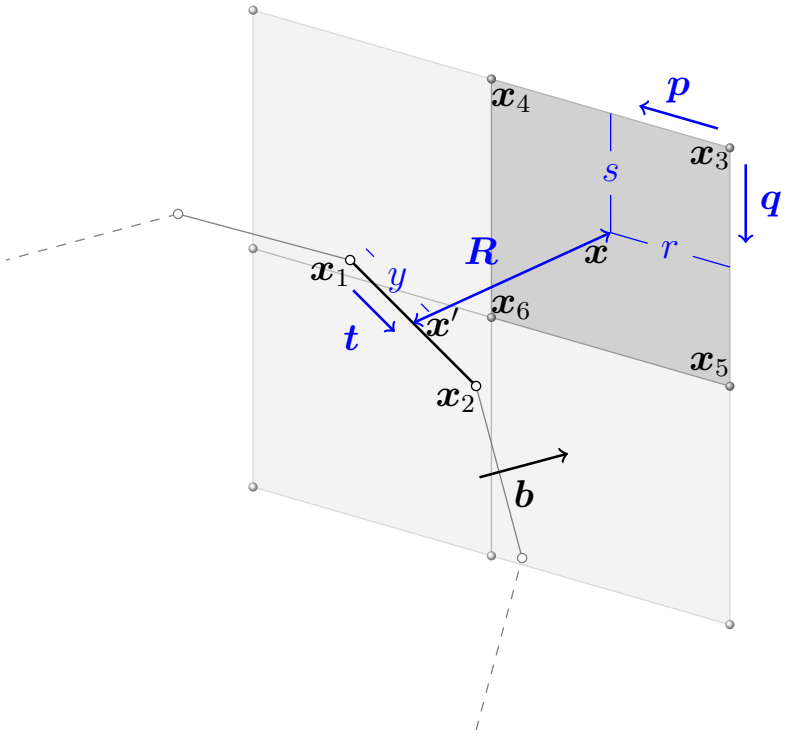

Figure 2: Geometry and associated variables for interface traction integration

where $i+j=k-2$, and the common part of the integrands will hereafter be referred as I_{ijk}, i.e.

$$I_{ijk} = \frac{(\boldsymbol{R}\cdot\boldsymbol{e}_{12})^i\,(\boldsymbol{R}\cdot\boldsymbol{e}_3)^j}{R^k}.$$

The main effort of this work lies in solving these series of triple integrals. We find that with the analytical solutions of a few seed integrals, all other integrals in the spherical harmonics expansion can be calculated analytically through recurrence relations. In Fig. 3, the required triple integrals for the traction force calculation are indicated with a blue color, and the rest triple integrals are necessary for the recursive integration to reach the required triple integrals of the same expansion order q and the next expansion order $q+1$. As illustrated by the blue dashed lines in Fig. 3, the double integrals at the intermediate levels are needed for the calculations of the triple integrals at the highest levels, and the single integrals at the lowest levels must be used to calculate the double integrals at the intermediate levels.

The required recurrence relations are constructed using the following partial derivatives:

$$\partial_y I_{ijk} = i\alpha I_{(i-1)jk} + j\phi I_{i(j-1)k} - k\,(\boldsymbol{R}\cdot\mathbf{t})\,I_{ij(k-2)} \tag{17}$$

$$\partial_r I_{ijk} = i\beta I_{(i-1)jk} + j\theta I_{i(j-1)k} - k\,(\boldsymbol{R}\cdot\mathbf{p})\,I_{ij(k-2)} \tag{18}$$

$$\partial_s I_{ijk} = i\gamma I_{(i-1)jk} + j\psi I_{i(j-1)k} - k\,(\boldsymbol{R}\cdot\mathbf{q})\,I_{ij(k-2)} \tag{19}$$

$$\partial_y\,(yI_{ijk}) = I_{ijk} + y\,\partial_y I_{ijk} \tag{20}$$

$$\partial_r\,(rI_{ijk}) = I_{ijk} + r\,\partial_r I_{ijk} \tag{21}$$

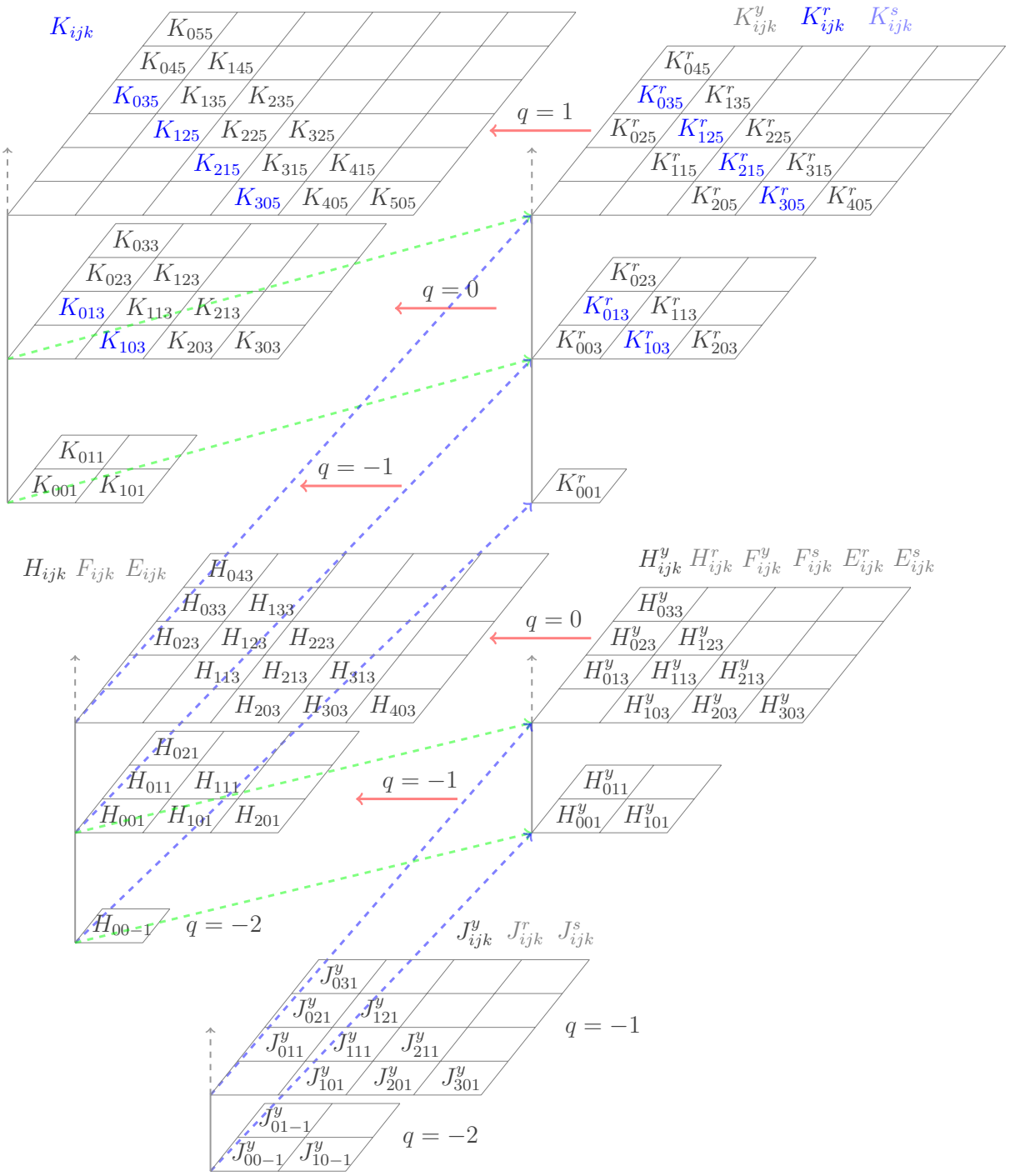

Figure 3: Interface traction integration through hierarchical recurrence relations

$$\partial_s\left(sI_{ijk}\right) = I_{ijk} + s\,\partial_s I_{ijk} \tag{22}$$
$$\partial_y\left(\boldsymbol{R}\cdot\mathbf{t}I_{ijk}\right) = I_{ijk} + \boldsymbol{R}\cdot\mathbf{t}\,\partial_y I_{ijk} \tag{23}$$
$$\partial_r\left(\boldsymbol{R}\cdot\mathbf{p}I_{ijk}\right) = I_{ijk} + \boldsymbol{R}\cdot\mathbf{p}\,\partial_r I_{ijk} \tag{24}$$
$$\partial_s\left(\boldsymbol{R}\cdot\mathbf{q}I_{ijk}\right) = I_{ijk} + \boldsymbol{R}\cdot\mathbf{q}\,\partial_s I_{ijk} \tag{25}$$

where $\alpha = \boldsymbol{t}\cdot\boldsymbol{e}_{12}$, $\beta = \boldsymbol{p}\cdot\boldsymbol{e}_{12}$, $\gamma = \boldsymbol{q}\cdot\boldsymbol{e}_{12}$, $\phi = \boldsymbol{t}\cdot\boldsymbol{e}_3$, $\theta = \boldsymbol{p}\cdot\boldsymbol{e}_3$, and $\psi = \boldsymbol{q}\cdot\boldsymbol{e}_3$.

The first three recurrence relations Eq. (26), Eq. (27), and Eq. (28) for the triple integrals are obtained by successive integrations over y, r, and s of the partial derivatives Eq. (17), Eq. (18), and Eq. (19), respectively. Another two recurrence relations Eq. (29) and Eq. (30) can be verified by the triple integral definitions.

$$K^y_{ij(k+2)} + cK^r_{ij(k+2)} + dK^s_{ij(k+2)} = \frac{1}{k}\left[i\alpha K_{(i-1)jk} + j\phi K_{i(j-1)k} - E_{ijk}\right] \tag{26}$$
$$cK^y_{ij(k+2)} + K^r_{ij(k+2)} + fK^s_{ij(k+2)} = \frac{1}{k}\left[i\beta K_{(i-1)jk} + j\theta K_{i(j-1)k} - F_{ijk}\right] \tag{27}$$
$$dK^y_{ij(k+2)} + fK^r_{ij(k+2)} + K^s_{ij(k+2)} = \frac{1}{k}\left[i\gamma K_{(i-1)jk} + j\psi K_{i(j-1)k} - H_{ijk}\right] \tag{28}$$
$$K_{(i+1)jk} = \alpha K^y_{ijk} + \beta K^r_{ijk} + \gamma K^s_{ijk} \tag{29}$$
$$K_{i(j+1)k} = \phi K^y_{ijk} + \theta K^r_{ijk} + \psi K^s_{ijk}, \tag{30}$$

where $c = \boldsymbol{p}\cdot\boldsymbol{t}$, $d = \boldsymbol{q}\cdot\boldsymbol{t}$, $f = \boldsymbol{p}\cdot\boldsymbol{q}$, $K^y_{ijk} = \int_{s_1}^{s_2}\int_{r_1}^{r_2}\int_{y_1}^{y_2} I_{ijk}y\mathrm{d}y\mathrm{d}r\mathrm{d}s$, $E_{ijk} = \int_{s_1}^{s_2}\int_{r_1}^{r_2} I_{ijk}\mathrm{d}r\mathrm{d}s$, $F_{ijk} = \int_{s_1}^{s_2}\int_{y_1}^{y_2} I_{ijk}\mathrm{d}y\mathrm{d}s$, and $H_{ijk} = \int_{r_1}^{r_2}\int_{y_1}^{y_2} I_{ijk}\mathrm{d}y\mathrm{d}r$. The double integrals H_{ijk}, F_{ijk}, and E_{ijk} need to be previously calculated using the second set of recurrence relations given below.

The first two recurrence relations Eq. (31) and Eq. (32) for the double integrals H_{ijk} are obtained by successive integrations over y and r of the partial derivatives Eq. (17) and Eq. (18), respectively. The third recurrence relation Eq. (33) for the double integrals H_{ijk} is obtained by successive integrations over y and r of the partial derivatives Eq. (20) and Eq. (21), and then summation of these two integration equations. Another two recurrence relations Eq. (34) and Eq. (35) can be verified by the double integral definitions. Analogously, the recurrence relations for the double integrals F_{ijk} Eq. (36) to Eq. (40) and for the double integrals E_{ijk} Eq. (41) to Eq. (45) are obtained using the corresponding partial derivatives and double integral definitions.

$$H^y_{ij(k+2)} + cH^r_{ij(k+2)} + dsH_{ij(k+2)} = \frac{1}{k}\left[i\alpha H_{(i-1)jk} + j\phi H_{i(j-1)k} - J^r_{ijk}\right] \tag{31}$$
$$cH^y_{ij(k+2)} + H^r_{ij(k+2)} + fsH_{ij(k+2)} = \frac{1}{k}\left[i\beta H_{(i-1)jk} + j\theta H_{i(j-1)k} - J^y_{ijk}\right] \tag{32}$$
$$\begin{aligned} dsH^y_{ij(k+2)} + fsH^r_{ij(k+2)} + s^2H_{ij(k+2)} = \tfrac{1}{k}\big[&i\gamma sH_{(i-1)jk} + j\psi sH_{i(j-1)k} \\ &+ (k-i-j-2)\,H_{ijk} + rJ^y_{ijk} + yJ^r_{ijk}\big] \end{aligned} \tag{33}$$
$$H_{(i+1)jk} = \alpha H^y_{ijk} + \beta H^r_{ijk} + \gamma sH_{ijk} \tag{34}$$
$$H_{i(j+1)k} = \phi H^y_{ijk} + \theta H^r_{ijk} + \psi sH_{ijk} \tag{35}$$
$$F^y_{ij(k+2)} + dF^s_{ij(k+2)} + crF_{ij(k+2)} = \frac{1}{k}\left[i\alpha F_{(i-1)jk} + j\phi F_{i(j-1)k} - J^s_{ijk}\right] \tag{36}$$
$$dF^y_{ij(k+2)} + F^s_{ij(k+2)} + frF_{ij(k+2)} = \frac{1}{k}\left[i\gamma F_{(i-1)jk} + j\psi F_{i(j-1)k} - J^y_{ijk}\right] \tag{37}$$

$$crF^{y}_{ij(k+2)} + frF^{s}_{ij(k+2)} + r^2F_{ij(k+2)} = \frac{1}{k}\left[i\beta rF_{(i-1)jk} + j\theta rF_{i(j-1)k} + (k-i-j-2)\,F_{ijk} + yJ^{s}_{ijk} + sJ^{y}_{ijk}\right] \tag{38}$$

$$F_{(i+1)jk} = \alpha F^{y}_{ijk} + \beta rF_{ijk} + \gamma F^{s}_{ijk} \tag{39}$$

$$F_{i(j+1)k} = \phi F^{y}_{ijk} + \theta rF_{ijk} + \psi F^{s}_{ijk} \tag{40}$$

$$E^{r}_{ij(k+2)} + fE^{s}_{ij(k+2)} + cyE_{ij(k+2)} = \frac{1}{k}\left[i\beta E_{(i-1)jk} + j\theta E_{i(j-1)k} - J^{s}_{ijk}\right] \tag{41}$$

$$fE^{r}_{ij(k+2)} + E^{s}_{ij(k+2)} + dyE_{ij(k+2)} = \frac{1}{k}\left[i\gamma E_{(i-1)jk} + j\psi E_{i(j-1)k} - J^{r}_{ijk}\right] \tag{42}$$

$$cyE^{r}_{ij(k+2)} + dyE^{r}_{ij(k+2)} + y^2E_{ij(k+2)} = \frac{1}{k}\left[i\alpha yE_{(i-1)jk} + j\phi yE_{i(j-1)k} + (k-i-j-2)\,E_{ijk} + sJ^{r}_{ijk} + rJ^{s}_{ijk}\right] \tag{43}$$

$$E_{(i+1)jk} = \alpha yE_{ijk} + \beta E^{r}_{ijk} + \gamma E^{s}_{ijk} \tag{44}$$

$$E_{i(j+1)k} = \phi yE_{ijk} + \theta E^{r}_{ijk} + \psi E^{s}_{ijk}, \tag{45}$$

where $H^{y}_{ijk} = \int_{r_1}^{r_2}\int_{y_1}^{y_2} I_{ijk}y\mathrm{d}y\mathrm{d}r$, $H^{r}_{ijk} = \int_{r_1}^{r_2}\int_{y_1}^{y_2} I_{ijk}r\mathrm{d}y\mathrm{d}r$, $F^{y}_{ijk} = \int_{s_1}^{s_2}\int_{y_1}^{y_2} I_{ijk}y\mathrm{d}y\mathrm{d}s$, $F^{s}_{ijk} = \int_{s_1}^{s_2}\int_{y_1}^{y_2} I_{ijk}s\mathrm{d}y\mathrm{d}s$, $E^{r}_{ijk} = \int_{s_1}^{s_2}\int_{r_1}^{r_2} I_{ijk}r\mathrm{d}r\mathrm{d}s$, $E^{s}_{ijk} = \int_{s_1}^{s_2}\int_{r_1}^{r_2} I_{ijk}s\mathrm{d}r\mathrm{d}s$, $J^{y}_{ijk} = \int_{y_1}^{y_2} I_{ijk}\mathrm{d}y$, $J^{r}_{ijk} = \int_{r_1}^{r_2} I_{ijk}\mathrm{d}r$, and $J^{s}_{ijk} = \int_{s_1}^{s_2} I_{ijk}\mathrm{d}s$. The single integrals J^{y}_{ijk}, J^{r}_{ijk}, and J^{s}_{ijk} must be formerly calculated using the third set of recurrence relations given below.

The first two recurrence relations Eq. (46) and Eq. (47) for the single integrals J^{y}_{ijk} are obtained by integration over y of the partial derivative Eq. (17) and multiplying both sides of the integration equation by α and ϕ, respectively. The third recurrence relation for the single integrals J^{y}_{ijk} Eq. (48) is obtained by integration over y of the partial derivative Eq. (23). Analogously, the recurrence relations for the single integrals J^{r}_{ijk} (from Eq. (49) to Eq. (51)) and J^{s}_{ijk} (from Eq. (52) to Eq. (54)) are obtained using the corresponding partial derivatives.

$$J^{y}_{(i+1)j(k+2)} = \frac{\alpha}{k}\left[i\alpha J^{y}_{(i-1)jk} + j\phi J^{y}_{i(j-1)k} - I_{ijk}\right] + J^{y}_{ij(k+2)}\left[(\beta-\alpha c)\,r + (\gamma-\alpha d)\,s\right] \tag{46}$$

$$J^{y}_{i(j+1)(k+2)} = \frac{\phi}{k}\left[i\alpha J^{y}_{(i-1)jk} + j\phi J^{y}_{i(j-1)k} - I_{ijk}\right] + J^{y}_{ij(k+2)}\left[(\theta-\phi c)\,r + (\psi-\phi d)\,s\right] \tag{47}$$

$$J^{y}_{ij(k+2)} = \frac{1}{k\left[R^2-(\boldsymbol{R}\cdot\mathbf{t})^2\right]}\Big[\boldsymbol{R}\cdot\mathbf{t}I_{ijk} + i\left[(\beta-\alpha c)\,r + (\gamma-\alpha d)\,s\right]J^{y}_{(i-1)jk} + j\left[(\theta-\phi c)\,r + (\psi-\phi d)\,s\right]J^{y}_{i(j-1)k} + (k-1-i-j)\,J^{y}_{ijk}\Big] \tag{48}$$

$$J^{r}_{(i+1)j(k+2)} = \frac{\beta}{k}\left[i\beta J^{r}_{(i-1)jk} + j\theta J^{r}_{i(j-1)k} - I_{ijk}\right] + J^{r}_{ij(k+2)}\left[(\alpha-\beta c)\,y + (\gamma-\beta f)\,s\right] \tag{49}$$

$$J^{r}_{i(j+1)(k+2)} = \frac{\theta}{k}\left[i\beta J^{r}_{(i-1)jk} + j\theta J^{r}_{i(j-1)k} - I_{ijk}\right] + J^{r}_{ij(k+2)}\left[(\phi-\theta c)\,y + (\psi-\theta f)\,s\right] \tag{50}$$

$$J^{r}_{ij(k+2)} = \frac{1}{k\left[R^2-(\boldsymbol{R}\cdot\mathbf{p})^2\right]}\Big[\boldsymbol{R}\cdot\mathbf{p}I_{ijk} + i\left[(\alpha-\beta c)\,y + (\gamma-\beta f)\,s\right]J^{r}_{(i-1)jk} + j\left[(\phi-\theta c)\,y + (\psi-\theta f)\,s\right]J^{r}_{i(j-1)k} + (k-1-i-j)\,J^{r}_{ijk}\Big] \tag{51}$$

$$J^{s}_{(i+1)j(k+2)} = \frac{\gamma}{k}\left[i\gamma J^{s}_{(i-1)jk} + j\psi J^{s}_{i(j-1)k} - I_{ijk}\right] + J^{s}_{ij(k+2)}\left[(\alpha-\gamma d)\,y + (\beta-\gamma f)\,r\right] \tag{52}$$

$$J^{s}_{i(j+1)(k+2)} = \frac{\psi}{k}\left[i\gamma J^{s}_{(i-1)jk} + j\psi J^{s}_{i(j-1)k} - I_{ijk}\right] + J^{s}_{ij(k+2)}\left[(\phi-\psi d)\,y + (\theta-\psi f)\,r\right] \tag{53}$$

$$J^s_{ij(k+2)} = \frac{1}{k\left[R^2-(\boldsymbol{R}\cdot\mathbf{q})^2\right]}\Big[\boldsymbol{R}\cdot\mathbf{q}I_{ijk} + i\left[(\alpha-\gamma d)\,y + (\beta-\gamma f)\,r\right]J^s_{(i-1)jk} + j\left[(\phi-\psi d)\,y + (\theta-\psi f)\,r\right]J^s_{i(j-1)k} + (k-1-i-j)\,J^s_{ijk}\Big] \tag{54}$$

As illustrated in Fig. 3, a number of seed integrals have to be first calculated before starting the recursive integrations. The seed single integrals J^y_{00-1}, J^r_{00-1}, and J^s_{00-1} can be directly calculated using the corresponding analytical solutions Eq. (55), Eq. (56), and Eq. (57), respectively.

$$J^y_{00-1} = \frac{1}{2}\left\{\left[R^2-(\boldsymbol{R}\cdot\mathbf{t})^2\right]\ln\left(R+\boldsymbol{R}\cdot\mathbf{t}\right)+\boldsymbol{R}\cdot\mathbf{t}R\right\} \tag{55}$$

$$J^r_{00-1} = \frac{1}{2}\left\{\left[R^2-(\boldsymbol{R}\cdot\mathbf{p})^2\right]\ln\left(R+\boldsymbol{R}\cdot\mathbf{p}\right)+\boldsymbol{R}\cdot\mathbf{p}R\right\} \tag{56}$$

$$J^s_{00-1} = \frac{1}{2}\left\{\left[R^2-(\boldsymbol{R}\cdot\mathbf{q})^2\right]\ln\left(R+\boldsymbol{R}\cdot\mathbf{q}\right)+\boldsymbol{R}\cdot\mathbf{q}R\right\} \tag{57}$$

The rest single integrals are all calculated using the recurrence relations Eq. (46) to Eq. (54). For each type of single integrals, the three recurrence relations are used to increase i, j, and k indices, respectively, e.g. $J^y_{00-1} \to J^y_{10-1}$, $J^y_{00-1} \to J^y_{01-1}$, and $J^y_{00-1} \to J^y_{001}$.

The seed double integrals H_{001}, H_{00-1}, F_{001}, F_{00-1}, E_{001}, and E_{00-1} are calculated using the analytical solution of H_{003}, F_{003}, and E_{003} given in Eq. (58), Eq. (59), and Eq. (60) and applying inverse recurrence relations Eq. (61), Eq. (62), and Eq. (63). These inverse recurrence relations are obtained by solving the first three recurrence relations for each type of the double integrals, i.e. Eq. (31) to Eq. (33) for H_{ijk}, Eq. (36) to Eq. (38) for F_{ijk}, and Eq. (41) to Eq. (43) for E_{ijk}.

$$H_{003} = \frac{2}{\sqrt{s^2(1+2cdf-c^2-d^2-f^2)}}\arctan\left[\frac{(1-c)(R+y-r)+(d-f)s}{\sqrt{s^2(1+2cdf-c^2-d^2-f^2)}}\right] \tag{58}$$

$$F_{003} = \frac{2}{\sqrt{r^2(1+2cdf-c^2-d^2-f^2)}}\arctan\left[\frac{(1-d)(R+y-s)+(c-f)r}{\sqrt{r^2(1+2cdf-c^2-d^2-f^2)}}\right] \tag{59}$$

$$E_{003} = \frac{2}{\sqrt{y^2(1+2cdf-c^2-d^2-f^2)}}\arctan\left[\frac{(1-f)(R+r-s)+(c-d)y}{\sqrt{y^2(1+2cdf-c^2-d^2-f^2)}}\right] \tag{60}$$

$$H_{00k} = \frac{1}{(k-2)(1-c^2)}\left\{k[(1-c^2)(1-d^2)-(f-cd)^2]s^2H_{00(k+2)} - [(1-c^2)r+(f-cd)s]J^y_{00k} - [(1-c^2)y+(d-cf)s]J^r_{00k}\right\} \tag{61}$$

$$F_{00k} = \frac{1}{(k-2)(1-d^2)}\left\{k[(1-c^2)(1-d^2)-(f-cd)^2]r^2F_{00(k+2)} - [(1-d^2)s+(f-cd)r]J^y_{00k} - [(1-d^2)y+(c-df)r]J^s_{00k}\right\} \tag{62}$$

$$E_{00k} = \frac{1}{(k-2)(1-f^2)}\left\{k[(1-c^2)(1-f^2)-(d-cf)^2]y^2E_{00(k+2)} - [(1-f^2)s+(d-cf)y]J^r_{00k} - [(1-f^2)r+(c-df)y]J^s_{00k}\right\} \tag{63}$$

The other double integrals are all calculated using the recurrence relations Eq. (31) to Eq. (45). The first three recurrences Eq. (31) to Eq. (33) are used to calculate the double integrals H^y_{ijk+2} and H^r_{ijk+2} from the available double integrals H_{ijk} and single integrals J^y_{ijk} and J^r_{ijk} at a lower k index, see Fig. 3. The last two recurrence relations Eq. (34) and Eq. (35) are used to calculate the double integrals H_{ijk} at higher i and j indices, respectively.

The seed triple integral K_{001} can be directly calculated from the seed double integrals H_{001}, F_{001}, and E_{001} using Eq. (64), which is obtained by successive integrations over y, r, and s of the partial derivatives Eq. (20), Eq. (21), and Eq. (22), and then summation of these three integration equations.

$$\begin{gathered}(3+i+j-k)\,K_{ijk} = yE_{ijk} + rF_{ijk} + sH_{ijk} \\ K_{001} = \tfrac{1}{2}\left(yE_{001} + rF_{001} + sH_{001}\right)\end{gathered} \tag{64}$$

The remaining triple integrals are all calculated using the recurrence relations Eq. (26) to Eq. (30). The first three recurrences Eq. (26) to Eq. (28) are used to calculated the double integrals K^{y}_{ijk+2}, K^{r}_{ijk+2}, and K^{s}_{ijk+2} from the available triple integrals K_{ijk} and the double integrals H_{ijk}, F_{ijk}, and E_{ijk} at a lower k index, see Fig. 3. The last two recurrence relations Eq. (29) and Eq. (30) are used to calculate the triple integrals K_{ijk} at higher i and j indices, respectively.

The triple integrals K^{rs}_{ijk} can be directly calculated from K_{ijk}, K^{r}_{ijk}, H^{r}_{ijk}, F_{ijk}, and E^{r}_{ijk} using the relations Eq. (65) to Eq. (67). The first equation is obtained by successive integrations over y, r, and s of the partial derivative Eq. (21). The last two equations are obtained by multiplying the partial differential equations Eq. (17) and Eq. (19) by r on both sides, and successive integrations over y, r, and s of these two partial differential equations, respectively.

$$K^{rr}_{ij(k+2)} + cK^{yr}_{ij(k+2)} + fK^{rs}_{ij(k+2)} = \frac{1}{k}\left[K_{ijk} + i\beta K^{r}_{(i-1)jk} + j\theta K^{r}_{i(j-1)k} - rF_{ijk}\right] \tag{65}$$

$$cK^{rr}_{ij(k+2)} + K^{yr}_{ij(k+2)} + dK^{rs}_{ij(k+2)} = \frac{1}{k}\left[i\alpha K^{r}_{(i-1)jk} + j\phi K^{r}_{i(j-1)k} - E^{r}_{ijk}\right] \tag{66}$$

$$fK^{rr}_{ij(k+2)} + dK^{yr}_{ij(k+2)} + K^{rs}_{ij(k+2)} = \frac{1}{k}\left[i\gamma K^{r}_{(i-1)jk} + j\psi K^{r}_{i(j-1)k} - H^{r}_{ijk}\right] \tag{67}$$

3 Results

To evaluate the accuracy and efficiency of our analytical traction force calculation, we perform q_{max} (spherical harmonics expansion order) convergence tests, and compare with Gaussian quadrature numerical integrations.

The infinite series of spherical harmonics expansions must be truncated in practice. Figure 4 shows how the relative error of the traction force calculation evolves as the spherical harmonics expansion order q_{max} increases. Similar to the dislocation interaction force calculations of Aubry and Arsenlis [51], the traction force calculations converge faster for materials with lower elastic anisotropy ratios, which means high orders of spherical harmonics expansion are needed for materials with high elastic anisotropy.

How the computation cost increases with the order of spherical harmonics expansion is presented in Fig. 5. The cost of our traction force calculation grows quadratically as the stress field calculation using the analytical expressions given in Ref. [51]. For the traction force calculation, using $q_{max} = 20$ is twenty times more expensive than using $q_{max} = 1$. The computation cost ratio between the traction force and stress field calculations is rather insensitive to the spherical harmonics expansion order, and changes from seven to six when q_{max} increases from one to twenty.

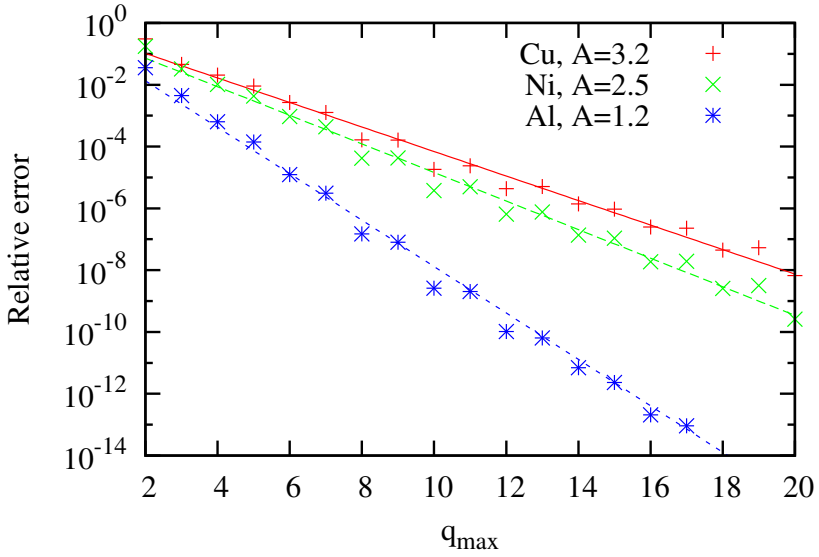

Figure 4: Convergence of traction force calculation as the spherical harmonics expansion order q_{max} increases for different materials in terms of the elastic anisotropy ratio A.

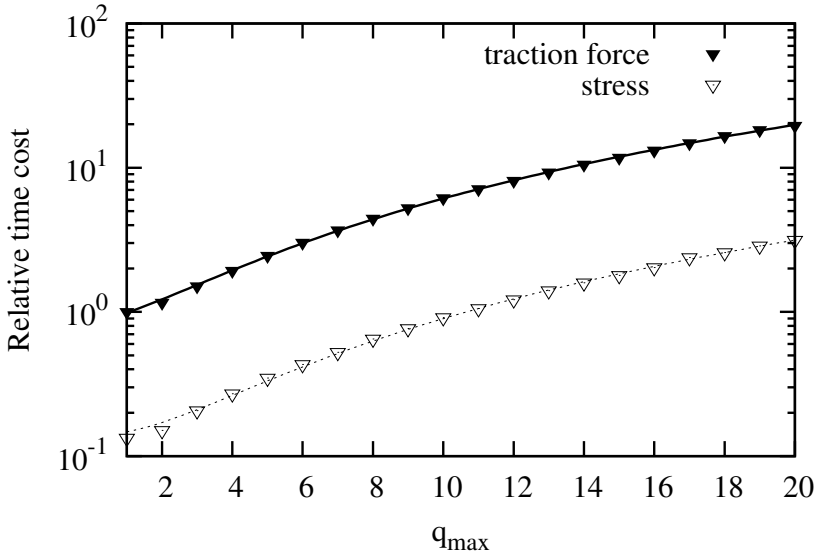

Figure 5: Quadratic computation cost growth of interface traction force and dislocation stress field calculations with the spherical harmonics expansion order q_{max}.

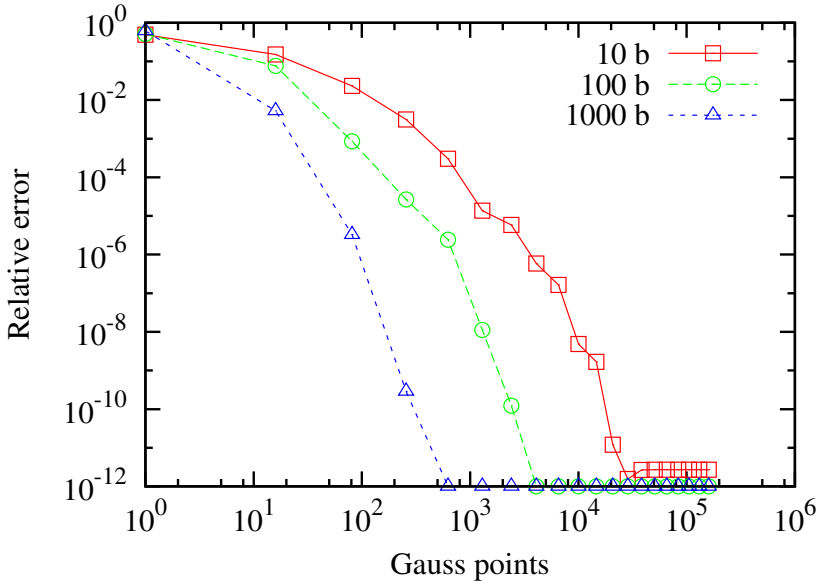

Figure 6: Comparison of Gaussian quadrature numerical integration and analytical triple integration using recurrence relations for Ni with $q_{max} = 10$ for different dislocation–interface distances in the unit of the Burgers vector's magnitude b.

We now compare our analytical interface traction force integrations with Gaussian quadrature numerical integrations using the analytical stress field expressions of Ref. [51]. As both the traction force and stress field calculations use the same spherical harmonics expansions of the derivatives of Green's function, the comparison of analytical and numerical integrations for a fixed q_{max} is roughly the same when q_{max} is changed from one to twenty.

Figure 6 depicts how the relative error between analytical and numerical integrations varies as the number of Gauss quadrature points increases in the numerical integrations. Similar to the traction force calculations of Queyreau et al. [43] for isotropic elastic media, the relative error decreases faster for larger dislocation–interface distances as the number of Gauss points increases in the numerical integrations. While the analytical solution is used as a reference to assess the error in numerical integrations, the comparison with numerical integrations using a large number of Gauss points can verify the correct implementation of the analytical traction force integration.

Figure 7 illustrates the computation cost comparison of analytical and numerical traction force integrations. The analytical integration becomes more efficient when the number of Gauss points exceeds eight in the numerical integration. With eight Gauss points, the error of the numerical integration is above one percent for a large dislocation–interface distance of 1000 b, and above ten percent for smaller dislocation–interface distances of 100 b and 10 b, Fig. 6. Keep in mind that the traction force calculation is only for one dislocation segment and one interface element, and the computation error can escalate in DD–FE/BE simulations with larger numbers of dislocation segments and interface elements over many correlated time steps. As proposed by Weygand et al. [20], a minimum of one hundred integration points has to be used for numerical integrations of surface traction forces. As shown in Fig. 7, compared with a numerical integra-

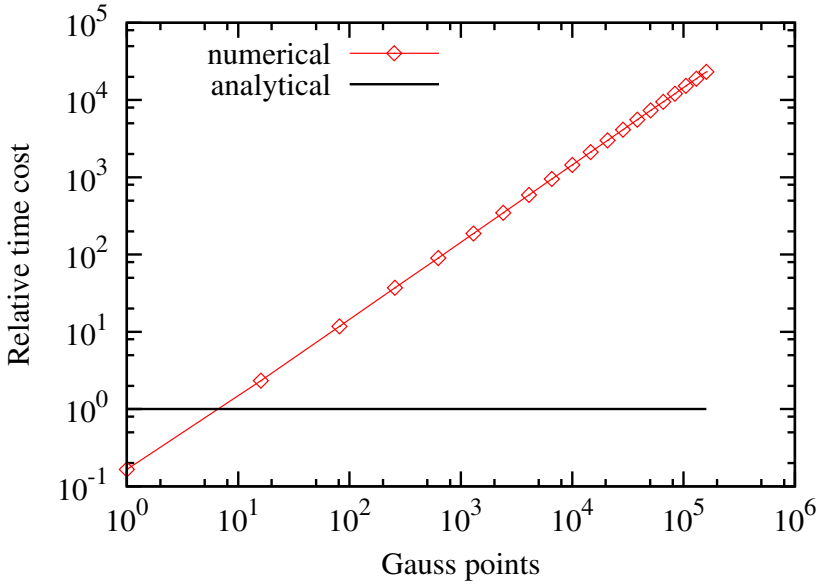

Figure 7: Computation cost comparison of Gaussian quadrature numerical integration and analytical triple integration using recurrence relations for a fixed q_{max} of 10.

tion using one hundred integration points, our analytical integration is more than one order of magnitude faster in speed.

Despite the obvious advantages of the analytical interface traction force integration, the algorithm implementation into a specific DD-FE/BE code can bring a considerable overhead to a short research project. In such a case, using simpler analytical stress field expressions and standard Gaussian quadrature numerical integrations may be preferred. Figure 8 shows how the computation error and cost of numerical integration varies with the number of Gauss points and the order of spherical harmonics expansion used in the stress field expressions. The numerical integration error is evaluated with respect to an analytical traction force integration using $q_{max} = 20$ for Ni with a dislocation–interface distance of 100 b. As can be seen in Fig. 8, there are optimized combinations of integration point number and spherical harmonics expansion order to achieve a desired level of accuracy, and it is often more efficient to increase the order of spherical harmonics expansion than the number of Gauss integration points.

4 Concluding remarks

Using spherical harmonics expansions of the derivatives of Green's function, we constructed the expressions for the interface traction force exerted by dislocation stress field in anisotropic elastic media, and develop hierarchical recurrence relations to integrate the spherical harmonics series to calculate the traction force. It is found that all the triples integrals associated with the spherical harmonics are functions of a few analytically solvable seed integrals. Compared with numerical integrations of the traction force, our analytical integrations have gained substantially

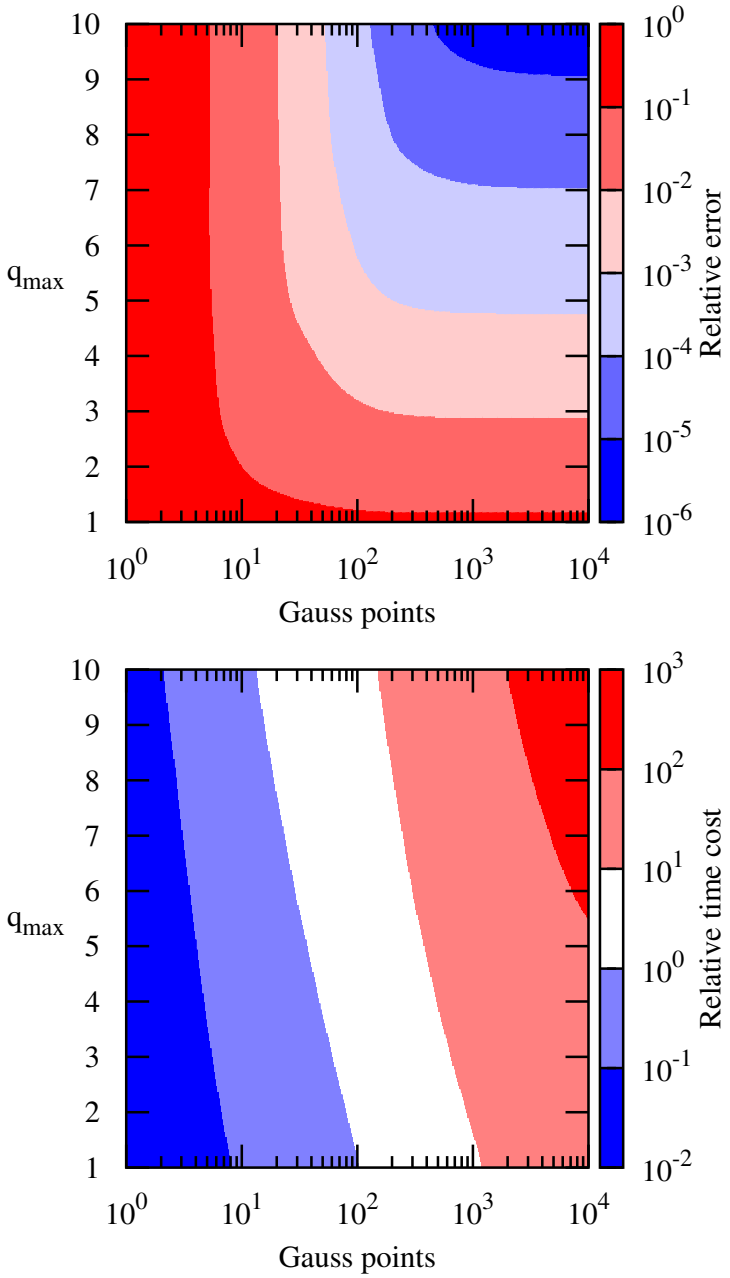

Figure 8: Computation error and time cost of numerical integrations with respect to an analytical traction force integration using $q_{max} = 20$.

in computation precision and speed. This development of analytical interface traction integrations can impart accuracy and efficiency to DD–FE/BE simulations of the elastic interactions between dislocations and interfaces in general elastically anisotropic crystalline materials.

Acknowledgments

We thank Sylvain Queyreau for helpful discussions. This work was performed under the auspices of the U.S. Department of Energy by Lawrence Livermore National Laboratory under Contract DE-AC52-07NA27344. Research was sponsored by the Army Research Laboratory and was accomplished under Cooperative Agreement Number W911NF-12-2-0022. The views and conclusions contained in this document are those of the authors and should not be interpreted as representing the official policies, either expressed or implied, of the Army Research Laboratory or the U.S. Government. The U.S. Government is authorized to reproduce and distribute reprints for Government purposes notwithstanding any copyright notation herein.

References

[1] Hull D. and Bacon D.J., 2011. *Introduction to Dislocations*. Butterworth-Heinemann, Oxford.

[2] Hirth J.P., 1972. The Influence of Grain Boundaries on Mechanical Properties. *Metall. Trans.*, 3:3047–3067.

[3] Sutton A.P. and Balluffi R.W., 1995. *Interfaces in Crystalline Materials*. Oxford University Press, Oxford.

[4] Priester L., 2013. *Grain Boundaries: From Theory to Engineering*. Springer, Dordrecht.

[5] Shan Z.W., Mishra R.K., Asif S.A.S., Warren O.L., and Minor A.M., 2008. Mechanical annealing and source-limited deformation in submicrometre-diameter Ni crystals. *Nature Mater.*, 7(2):115–119.

[6] Oh S.H., Legros M., Kiener D., and Dehm G., 2009. In situ observation of dislocation nucleation and escape in a submicrometre aluminium single crystal. *Nature Mater.*, 8(2):95–100.

[7] Brinckmann S., Kim J.Y., and Greer J.R., 2008. Fundamental differences in mechanical behavior between two types of crystals at the nanoscale. *Phys. Rev. Lett.*, 100(15):155502.

[8] Weinberger C.R. and Cai W., 2008. Surface-controlled dislocation multiplication in metal micropillars. *Proc. Natl. Acad. Sci. USA*, 105(38):14304–14307.

[9] Gleiter H., 2000. Nanostructured materials: Basic concepts and microstructure. *Acta Mater.*, 48(1):1–29.

[10] Jin Z.H., Gumbsch P., Ma E., Albe K., Lu K., Hahn H., and Gleiter H., 2006. The interaction mechanism of screw dislocations with coherent twin boundaries in different face-centred cubic metals. *Scripta Mater.*, 54(6):1163–1168.

[11] Estrin Y., Lemiale V., O'Donnell R., and Toth L., 2011. On homogeneous nucleation of dislocation loops in nanocrystalline materials. *Metall. Mater. Trans. A*, 42A(13):3883–3888.

[12] Jang D., Li X., Gao H., and Greer J.R., 2012. Deformation mechanisms in nanotwinned metal nanopillars. *Nature Nanotech.*, 7(9):594–601.

[13] Barnett D.M. and Lothe J., 1974. An image force theorem for dislocations in anisotropic bicrystals. *J. Phys. F: Metal Phys.*, 4(10):1618.

[14] Belov A.Y., Chamrov V.A., Indenbom V.L., and Lothe J., 1983. Elastic fields of dislocations piercing the interface of an anisotropic bicrystal. *phys. stat. sol. (b)*, 119(2):565–578.

[15] Khalfallah O., Condat M., and Priester L., 1993. Image force on a lattice dislocation due to a grain boundary in b.c.c. metals. *Philos. Mag. A*, 67(1):231–250.

[16] Priester L. and Khalfallah O., 1994. Image force on a lattice dislocation due to a grain boundary in anisotropic f.c.c. materials. *Philos. Mag. A*, 69(3):471–484.

[17] Khalfallah O. and Priester L., 1999. Image force on a lattice dislocation due to a grain boundary in hexagonal metals. In Lejcek, P and Paidar, V (Ed.), *Intergranular and Interphase Boundaries in Materials*, volume 294-296 of *Mater. Sci. Forum*, pages 689–692.

[18] van der Giessen E. and Needleman A., 1995. Discrete dislocation plasticity: a simple planar model. *Modelling Simul. Mater. Sci. Eng.*, 3(5):689–735.

[19] Zbib H.M. and Diaz de la Rubia T., 2002. A multiscale model of plasticity. *Int. J. Plasticity,*, 18(9):1133–1163.

[20] Weygand D., Friedman L.H., Van der Giessen E., and Needleman A., 2002. Aspects of boundary-value problem solutions with three-dimensional dislocation dynamics. *Modelling Simul. Mater. Sci. Eng.*, 10(4):437–468.

[21] O'Day M.P. and Curtin W.A., 2004. A superposition framework for discrete dislocation plasticity. *J. Appl. Mech.*, 71(6):805–815.

[22] O'Day M.P. and Curtin W.A., 2005. Bimaterial interface fracture: A discrete dislocation model. *J. Mech. Phys. Solids*, 53(2):359–382.

[23] Tang M., Cai W., Xu G., and Bulatov V.V., 2006. A hybrid method for computing forces on curved dislocations intersecting free surfaces in three-dimensional dislocation dynamics. *Modelling Simul. Mater. Sci. Eng.*, 14(7):1139–1151.

[24] El-Awady J.A., Biner S.B., and Ghoniem N.M., 2008. A self-consistent boundary element, parametric dislocation dynamics formulation of plastic flow in finite volumes. *J. Mech. Phys. Solids*, 56(5):2019–2035.

[25] Deng J., El-Azab A., and Larson B.C., 2008. On the elastic boundary value problem of dislocations in bounded crystals. *Philos. Mag.*, 88(30-32):3527–3548.

[26] Shishvan S.S., Mohammadi S., Rahimian M., and Van der Giessen E., 2011. Plane-strain discrete dislocation plasticity incorporating anisotropic elasticity. *Int. J. Solids Struct.*, 48(2):374 – 387.

[27] Vattre A., Devincre B., Feyel F., Gatti R., Groh S., Jamond O., and Roos A., 2014. Modelling crystal plasticity by 3D dislocation dynamics and the finite element method: The Discrete-Continuous Model revisited. *J. Mech. Phys. Solids*, 63:491–505.

[28] Crone J.C., Chung P.W., Leiter K.W., Knap J., Aubry S., Hommes G., and Arsenlis A., 2014. A multiply parallel implementation of finite element-based discrete dislocation dynamics for arbitrary geometries. *Modelling Simul. Mater. Sci. Eng.*, 22(3):035014.

[29] Schwarz K.W., 1999. Simulation of dislocations on the mesoscopic scale. I. Methods and examples. *J. Appl. Phys.*, 85(1):108–119.

[30] Ghoniem N.M., Tong S.H., and Sun L.Z., 2000. Parametric dislocation dynamics: A thermodynamics-based approach to investigations of mesoscopic plastic deformation. *Phys. Rev. B*, 61(2):913–927.

[31] Arsenlis A., Cai W., Tang M., Rhee M., Oppelstrup T., Hommes G., Pierce T.G., and Bulatov V.V., 2007. Enabling strain hardening simulations with dislocation dynamics. *Modelling Simul. Mater. Sci. Eng.*, 15(6):553–595.

[32] Liu X.H., Ross F.M., and Schwarz K.W., 2000. Dislocated epitaxial islands. *Phys. Rev. Lett.*, 85(19):4088–4091.

[33] Weinberger C.R. and Cai W., 2007. Computing image stress in an elastic cylinder. *J. Mech. Phys. Solids*, 55(10):2027–2054.

[34] Fertig R.S. and Baker S.P., 2009. Simulation of dislocations and strength in thin films: A review. *Prog. Mater. Sci.*, 54(6):874–908.

[35] Hirth J.P. and Lothe J., 1982. *Theory of Dislocations*. Wiley, New York.

[36] Cai W., Arsenlis A., Weinberger C.R., and Bulatov V.V., 2006. A non-singular continuum theory of dislocations. *J. Mech. Phys. Solids*, 54(3):561–587.

[37] Bulatov V.V., Hsiung L.L., Tang M., Arsenlis A., Bartelt M.C., Cai W., Florando J.N., Hiratani M., Rhee M., Hommes G., Pierce T.G., and Diaz de la Rubia T., 2006. Dislocation multi-junctions and strain hardening. *Nature*, 440(7088):1174–1178.

[38] Rao S.I., Dimiduk D.M., Parthasarathy T.A., Uchic M.D., Tang M., and Woodward C., 2008. Athermal mechanisms of size-dependent crystal flow gleaned from three-dimensional discrete dislocation simulations. *Acta Mater.*, 56(13):3245–3259.

[39] Liu B., Raabe D., Eisenlohr P., Roters F., Arsenlis A., and Hommes G., 2011. Dislocation interactions and low-angle grain boundary strengthening. *Acta Mater.*, 59(19):7125–7134.

[40] Liu B., Eisenlohr P., Roters F., and Raabe D., 2012. Simulation of dislocation penetration through a general low-angle grain boundary. *Acta Mater.*, 60(13-14):5380–5390.

[41] Arsenlis A., Rhee M., Hommes G., Cook R., and Marian J., 2012. A dislocation dynamics study of the transition from homogeneous to heterogeneous deformation in irradiated body-centered cubic iron. *Acta Mater.*, 60(9):3748–3757.

[42] Liu B., Raabe D., Roters F., and Arsenlis A., 2014. Interfacial dislocation motion and interactions in single-crystal superalloys. *Acta Mater.*, 79:216–233.

[43] Queyreau S., Marian J., Wirth B.D., and Arsenlis A., 2014. Analytical integration of the forces induced by dislocations on a surface element. *Modelling Simul. Mater. Sci. Eng.*, 22(3):035004.

[44] Bacon D.J., Barnett D.M., and Scattergood R.O., 1980. Anisotropic continuum theory of lattice defects. *Prog. Mater. Sci.*, 23:51 – 262.

[45] Chu H.J., Pan E., Han X., Wang J., and Beyerlein I.J., 2012. Elastic fields of dislocation loops in three-dimensional anisotropic bimaterials. *J. Mech. Phys. Solids*, 60(3):418–431.

[46] Stroh A.N., 1962. Steady state problems in anisotropic elasticity. *J. Math. Phys.*, 41(2):77.

[47] Rhee M., Stolken J.S., Bulatov V.V., Diaz de la Rubia T., Zbib H.M., and Hirth J.P., 2001. Dislocation stress fields for dynamic codes using anisotropic elasticity: methodology and analysis. *Mater. Sci. Eng. A*, 309310(0):288 – 293.

[48] Yin J., Barnett D.M., and Cai W., 2010. Efficient computation of forces on dislocation segments in anisotropic elasticity. *Modelling Simul. Mater. Sci. Eng.*, 18(4):045013.

[49] Mura T., 1987. *Micromechanics of Defects in Solids*. Kluwer, Dordrecht.

[50] Han X., Ghoniem N.M., and Wang Z., 2003. Parametric dislocation dynamics of anisotropic crystals. *Philos. Mag.*, 83(31-34, SI):3705–3721.

[51] Aubry S. and Arsenlis A., 2013. Use of spherical harmonics for dislocation dynamics in anisotropic elastic media. *Modelling Simul. Mater. Sci. Eng.*, 21(6):065013.

[52] Barnett D.M., 1972. The precise evaluation of derivatives of the anisotropic elastic green's functions. *physica status solidi (b)*, 49(2):741–748.